Thermogravitational convection of ferrofluid combined with the second law of thermodynamics for an open chamber with a heat-generating solid block under an influence of uniform magnetic field

C. Sivaraj [a], E. Vignesh [a], M.A. Sheremet [b],[*]

[a] *Department of Mathematics, PSG College of Arts & Science, Coimbatore 641014, Tamil Nadu, India*
[b] *Laboratory on Convective Heat and Mass Transfer, Tomsk State University, 634050 Tomsk, Russia*

A R T I C L E   I N F O

A B S T R A C T

The present numerical study scrutinizes the effect of uniform Lorentz force on the thermogravitational energy transport and entropy production of nanosuspension in an open domain with a heat-generating solid element. The left border is kept at low temperature (T_c) whilst the horizontal borders are assumed to be adiabatic. Finite volume method (FVM) is employed to work out the heat and mass transfer equations. For fixed value of Rayleigh number ($Ra = 10^7$), numerical analysis was optimized for wide ranges of nanoparticle volume fraction ($\phi = 1\%$–4%), thermal conductivity ratio of a heat generating body ($k^* = 0.1$–5), Hartmann parameter ($Ha = 0$–100), angle of inclined magnetic field ($\gamma = 0°$–90°) and non-dimensional temperature drop ($\Omega = 0.001$–0.1). The numerical solutions were analyzed employing patterns of temperature and stream function as well as average Nusselt number and entropy lines. The outcomes indicated that, an increasing magnetic parameter Ha leads to reduction of mean Nu and the rate of entropy production. An addition of nano-sized particles enhances the energy transport and average entropy production for the system. It is also revealed that the maximum energy transport strength occurs at high thermal conductivity ratio ($k^* = 5$).

1. Introduction

Convective energy transmission in open cavities with heat generating solids is one of the essential fields in engineering and geophysical systems due to many various applications including electronic device cooling, mechanical engineering, heating or cooling of structures and solar energy generation. The basic examples are shown by Xie et al. [1]. In modern years nanosuspensions have bring an essential attention for energy removal in different engineering and industrial systems. This is due to the fact that nanoadditives which are characterized the highest thermal conductivity and system stability than base fluids. Nowadays, all electronic components consist of nano- or micro-sized electronic chips.

The major problem is related to heat transmission to optimize engineering devices will be. To tackle this problem and create an effective cooling system for reducing temperature additional techniques have been announced during last decades. Thus, Aminossadati and Ghasemi [2] investigated the mixed convective energy transport in a channel under different heating modes which is placed at different sides of the open cavity. They found that when the heater is placed on the right border, the chamber of a doubled aspect ratio is characterized by the maximum energy transport strength. The results also show that the cavity aspect ratio growth provides significant enhancement of the energy transport mode. Shuja et al. [3] analyzed thermogravitational energy transport in a chamber due to a protruding body. Authors showed that the average Nu is reduced when growing the aspect ratio of heated block and the overall irreversibility to energy transport ratio decreased with a raise of the aspect ratio. Rahman et al. [4] examined mixed convective energy transference in a ventilated chamber having a circular energy producing body. They found that mean Nu at the surfaces of body enhances as Re and Pr are increased. Singh and Singh [5] considered the study of conjugate thermal convection combined with thermal radiation in upper opened chamber. Their results showed that top zone of the left border is the efficient position of energy source for cooling a system.

Miroshnichenko et al. [6] scrutinized the thermogravitational energy transport of nanoliquid within an opened inclined chamber having a heat producing element. Authors found that the cavity titled angle of $\pi/3$ and central placed heater characterized the effective cooling of the system. Sheremet et al. [7] worked on thermogravitational energy

---

Nomenclature

Roman letters

A^*	solid body area ratio
B	magnitude of the uniform magnetic field
Be	Bejan number
Be_{avg}	mean Bejan number
g	gravitational acceleration
c_p	thermal capacity
Ge	Gebhart number
Ha	Hartmann number
k	heat conductivity
k^*	heat conductivity ratio
l	size of the solid block
L	size of the cavity
Nu	Nusselt number
$\overline{Nu}$	mean Nusselt number
p	pressure
P	non-dimensional pressure
Pr	Prandtl number
q'''	volume density of heat flux
Ra	Rayleigh number
$\overline{s_{gen}}$	local entropy generation
$\overline{s_T}$	local entropy generation induced by energy transport
$\overline{s_{T,f}}$	local entropy generation induced by heat transport for liquid
$\overline{s_{T,s}}$	local entropy generation induced by heat transport for solid
$\overline{s_F}$	local entropy generation induced by nanosuspension friction
$\overline{s_M}$	local entropy generation induced by Lorentz force
S_{gen}	dimensionless local entropy generation
S_T	dimensionless local entropy generation induced by heat transport
$S_{T,f}$	dimensionless local entropy generation induced by heat transport for liquid
$S_{T,s}$	dimensionless local entropy generation induced by heat transport for solid
S_F	dimensionless local entropy generation induced by

	nanosuspension friction
S_M	dimensionless local entropy generation induced by Lorentz force
$S_{gen,avg}$	dimensionless average entropy generation
$S_{T,avg}$	dimensionless average entropy generation induced by heat transport
$S_{F,avg}$	dimensionless average entropy generation induced by nanosuspension friction
$S_{M,avg}$	dimensionless local entropy generation induced by Lorentz force
t	time
T	temperature
T_c	temperature at cooled vertical border
u, v	velocity components at x- and y-coordinates
U, V	non-dimensional velocity projections
x, y	Cartesian coordinates
X, Y	non-dimensional Cartesian coordinates

Greek Symbols

α	thermal diffusivity
β	thermal expansion coefficient
γ	angle of inclined magnetic field
ν	kinematic viscosity
μ	dynamic viscosity
θ	non-dimensional temperature
ρ	density
ρc_p	thermal capacitance
σ	electrical conductivity
τ	non-dimensional time
ϕ	nano-sized particles concentration
Ψ	non-dimensional stream function
Ω	non-dimensional temperature drop

Subscripts

avg	average
c	cold
f	fluid
h	hot
nf	nanofluid
p	particle
s	solid

transport of nanoliquid inside an opened chamber with thermally-conducting solid border and heat-producing element. An inclusion of nano-sized alumina particles can decrease the mean temperature of the heater. Moreover, nanofluid is very useful in the case of low intensive flow. Mahmoudi et al. [8] made a computational analysis of thermal convection within an opened cabinet having two vertical thin energy elements under an influence of nanoliquid circulation. Authors noted that the heat and the fluid motion within the chamber are significantly influenced by Ra and the heater location. The results indicate that the increasing Ra augments the energy transport strength.

Oh et al. [9] examined thermogravitational energy transference within a closed chamber having an energy-producing solid block. They showed that the ratio of mean Nu at the heated border to that of the cooled border varies between −1 and 1. Raisi [10] scrutinized conjugate thermal convection in a region with a nanoliquid under an impact of energy-producing solid square body. He found that increasing Ra and concentration of nanoadditives improve the heat transmission within the domain. Shulepova et al. [11] investigated the mixed convective heat transference in a region with moved wall filled with nano-suspension under an impact of time-dependent energy-producing solid block with the effect of radiation. They revealed that an inclusion of nanoadditives characterizes a diminution of the source temperature, while liquid circulation strength reduces. The free convective energy

transport in a cavity having heated solid block under the influence of heat radiation was studied by Saravanan and Sivaraj [12]. They found that high surface emissivity and Ra can induce good energy transport strength under the isothermal and heat-generating elements. Mikhai-lenko et al. [13] conducted a numerical analysis on rotating chamber having energy-producing element under the radiative effect. The chamber rotation and optical parameters of the borders can be defined as governing aspects of the optimal passive cooling technique. Pop et al. [14] examined the thermal convection within a differentially warmed cavity having internal heat-insulated or heat-conducting body. Their result showed that high thermal conductivity of internal body illustrates a reduction of the average Nu. Moreover, non-monotonic impact on the mean Nu occurs at changing internal body size. Sivaraj et al. [15] studied the impact of surface emissivity on free convection in an inclined domain with energy-producing element. They found that the dominance of heat radiation on total energy transport is strong under an impact of walls emissivity of heat-generating block and chamber borders. Free convection in a three-dimensional cabinet with rectangular energy-producing element was studied computationally by Purusothaman et al. [16]. They revealed that enhancing Ra and aspect ratio of heat generating sources illustrate highly effective heat transfer performance in the domain.

Recently, the use of nanofluid with CNT for simulation of MHD
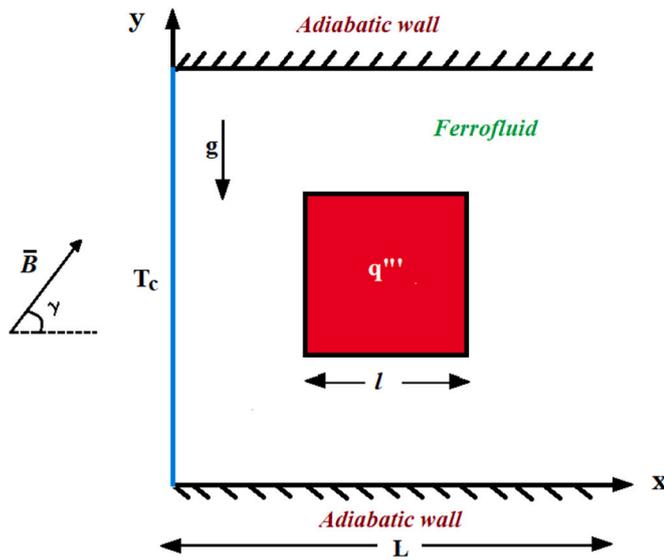
Fig. 1. Physical geometry.

Table 1

Thermo-physical attributes of the host liquid and solid nanoadditives [45,46].

Physical attributes	(Basefluid) H_2O	(Nanoparticles) Fe_3O_4
c_p [J kg^{-1} K^{-1}]	4179	670
ρ [kg m^{-3}]	997.1	5200
k [W m^{-1} K^{-1}]	0.613	6
$\beta \times 10^{-5}$ [K^{-1}]	20.7	1.18
σ [S m^{-1}]	0.05	25,000
μ [kg m^{-1} s^{-1}]	0.001003	–
Pr	6.8377	–

Table 2

Comparison of solutions with literatures for a square chamber with fully opened vertical side for $Pr = 1.0$.

Ra	$\overline{Nu}$		
	Chan and Tien [43]	Hinojosa et al. [44]	Present study
10^4	3.41	3.57	3.60
10^5	7.69	7.75	7.81
10^6	15.0	15.11	15.20
10^7	28.6	28.70	28.99

Table 3

Comparison of overall entropy production with data of [42].

Ω	0.02	0.04	0.06	0.08	0.1
Famouri and Hooman [42]	6.701	6.576	6.457	6.342	6.231
Present study	6.715	6.586	6.463	6.343	6.228

Table 4

Comparison of mean Nu with data of [55].

Ra	ζ	$\overline{Nu}$			
		k^*	House et al. [55]	Present study	Difference (%)
10^5	0.5	0.2	4.624	4.639	0.32
10^5	0.5	1.0	4.506	4.518	0.26
10^5	0.5	5.0	4.324	4.333	0.20
10^6	0.9	0.2	2.402	2.437	1.45
10^6	0.9	5.0	3.868	3.849	0.49

Table 5

Effect of mesh parameters.

Grid	62×62	122×122	182×182	242×242
$|\Psi|_{max}$	31.4004	32.0204	32.0210	32.8958

thermogravitational convection in a circular domain with heat-generating solid element was reported by Tayebi et al. [17]. They revealed that the total thermal transmission can be enhanced with Ra and heat conductivity parameter (Kr) and it reduces with increasing magnetic parameter and CNTs concentration. Also, augmenting Kr characterizes a reduction of the mean internal block temperature and the nanosuspension temperature rises. Gangawane [18] investigated MHD thermogravitational energy transport in a partially warmed open chamber. Analysis was focused on various values of heat sources size and magnetic parameter (Ha) with various angles of tilted magnetic influence. Author found that the increasing Ra and magnetic inclination at 45° provided the highest heat transfer. Abbassi [19] have numerically investigated MHD thermogravitational energy transport within an opened nanosuspension chamber having heat production or absorption. The author discussed that mean Nu rises with nanoadditives concentration when Brownian motion is considered and the energy production or absorption parameter is disappeared in the case of higher Rayleigh number. Mahmoudi et al. [20] conducted an investigation of free convection in an opened chamber with a non-uniform border restrictions under impact of magnetic field and uniform energy production or absorption. Authors revealed that the energy transport strength is weakened with increase of Ha and can be enhanced with a growth of Ra. Also, the nanosuspension effect is more essential at high Ra. Prakash et al. [21] conducted a computational investigation to study the effect of energy generation on MHD natural convective liquid motion within a vertical duct under an influence of changeable properties. They explored the behavior of fluid velocity and temperature and analyzed the effect of magnetic and heat production effect. Rahman et al. [22] numerically studied MHD mixed convection inside a closed domain with moved borders under an impact of inner energy-producing body. They concluded that for the highest heat generating parameter the maximum liquid temperature within the chamber can be found, while the temperature at the cylinder center and the flow rates are increased. Sivaraj and Sheremet [23] examined MHD free convection in a tilted porous chamber having internal solid block. The authors have shown that a rise of Ha reduces the fluid flow rate in the cavity. Also, a non-linear change of mean Nu can be found with an increasing angle of inclined magnetic influence. Alsabery et al. [24] numerically studied the mixed convection in a region with moving wall under the influence of inner solid body, tilted Lorentz force and corner heater. They found that a large size of the solid body can increase thermal performance for high Re and Ri. Job and Gunakala [25] studied the unsteady MHD mixed convective motion of hybrid nanofluids within a horizontal grooved duct having two energy-producing solid cylinders. Authors reported that the rate of energy transport enhances with a rise of magnetic parameter and the thermal transmission rate was found to be maximum for alumina-water nanofluid at low Re.

Ahmed et al. [26] studied computationally MHD mixed convective thermal transference in a tilted chamber filled with Cu/H_2O nanosuspension under the heat production, partial slip and adiabatic block influences. For low value of magnetic parameter they ascertained that an inclusion of nanoadditives leads to better energy transport. Also, increasing Hartmann number can weaken the fluid flow rate. MHD and energy production influence on time-dependent free convection in a porous domain was calculated by Revnic et al. [27]. They demonstrated that with raising Ha, also for high Ra, the diffusive thermal transfer become eminent. Ali et al. [28] scrutinized the buoyancy driven convection in a hybrid nanosuspension irregular chamber having energy-producing cylindrical block. Authors found that the fluid flow becomes higher for wavy cavity having heat generating body than smooth
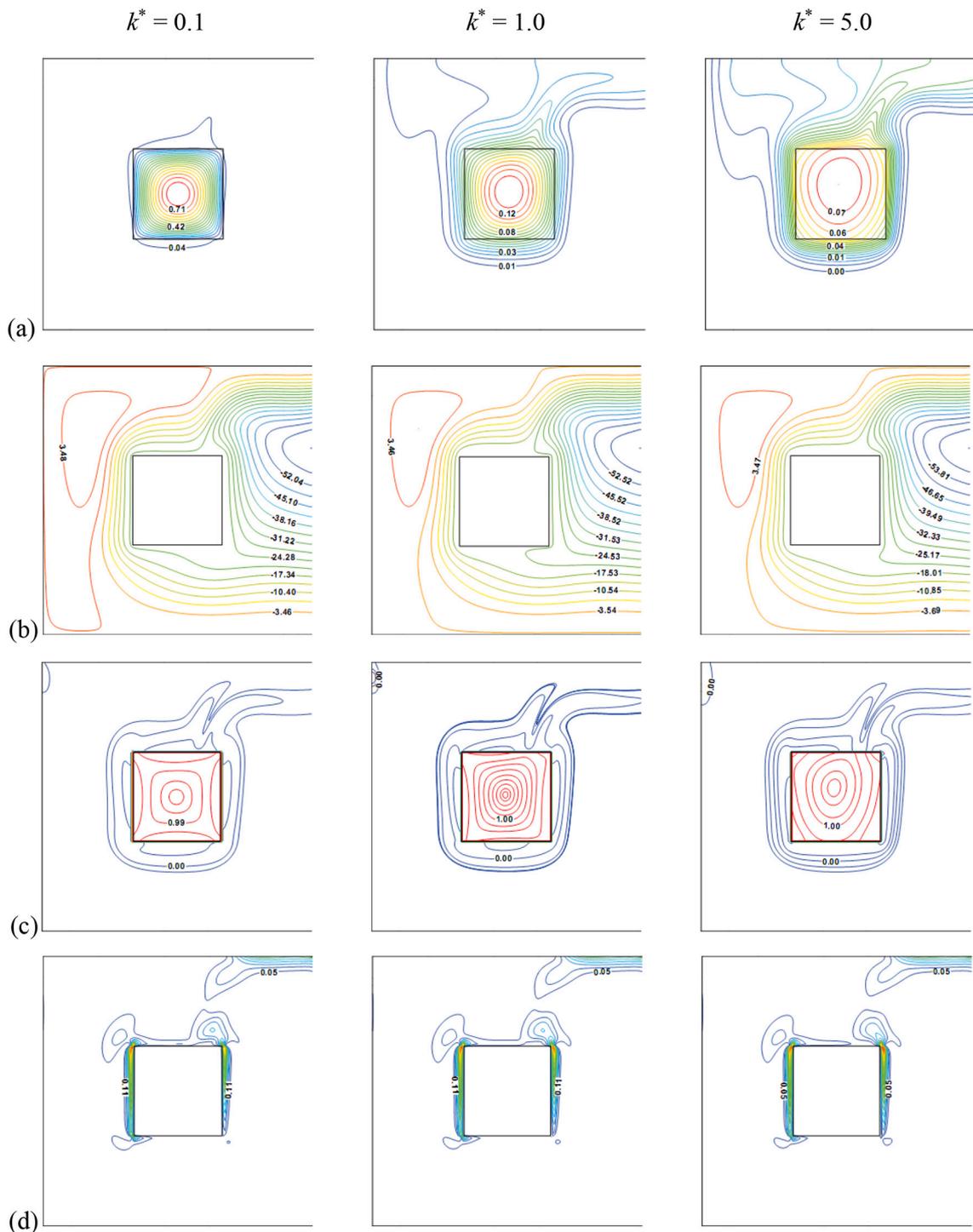
Fig. 2. Patterns of θ (a), Ψ (b), S_T (c), S_F (d) for ϕ = 0.04, Ω = 0.01 and Ha = 0 with various k^*.

cavity without heat generating obstacles. Also, lower heater length and radius of the heat generating cylinder provide better heat transfer. Saha [29] studied the effect of magnetic field and energy production on thermal convective circulation within an opened chamber with the microgravity influence. It was observed that the energy transport strength is reduced with a raise of the magnetic Ra and the paramagnetic liquid coefficient.

Entropy generation can give better details about energy dropping due to irreversibility of heat transference and nanosuspension friction, so that heat is retaining by minimizing this loss. Thus, Shuja and Yilbas [30] scrutinized the free convection combined with the second law of

thermodynamics in an opened chamber having porous block. Authors demonstrated that raising aspect ratio and porosity of the body reduce the total entropy production intensity in the domain. Hosseini et al. [31] considered MHD and entropy generation on a symmetrically heated horizontal porous microchannel filled with nanofluid containing heat generating solid body. Authors ascertained that the solid and fluid energy transport irreversibilities are weakened with magnetic impact which demonstrates the favor to magnetic field in turn down the energy transport irreversibility. Shuja et al. [32] investigated the usage of the second law of thermodynamics for free convection in a square chamber having energy producing solid block. Authors indicated that the location
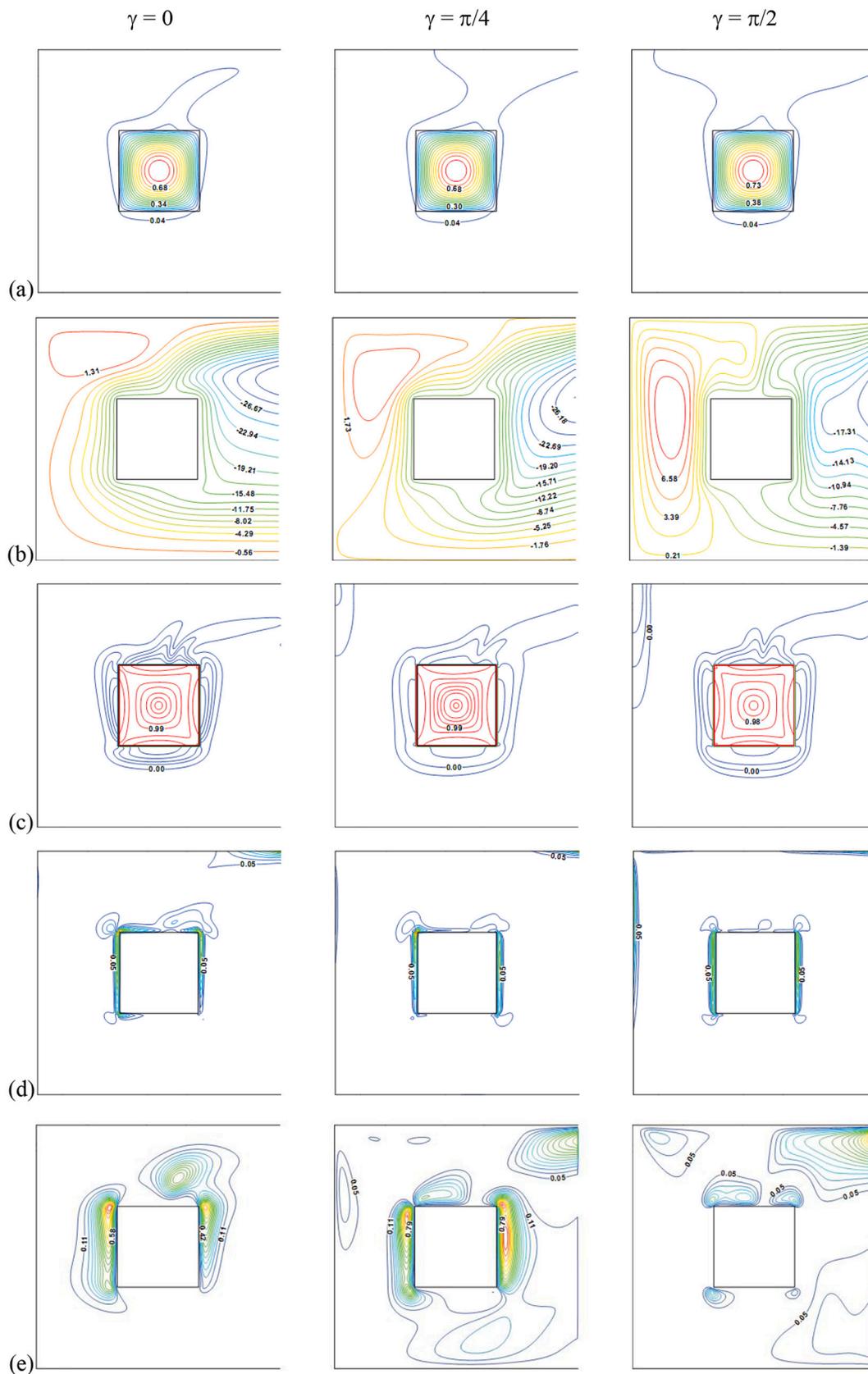
Fig. 3. Patterns of θ (a), Ψ (b), S_T (c), S_F (d) and S_M (e) for $k* = 0.1$, $\phi = 0.04$, $\Omega = 0.01$ and $Ha = 50$ with various γ.
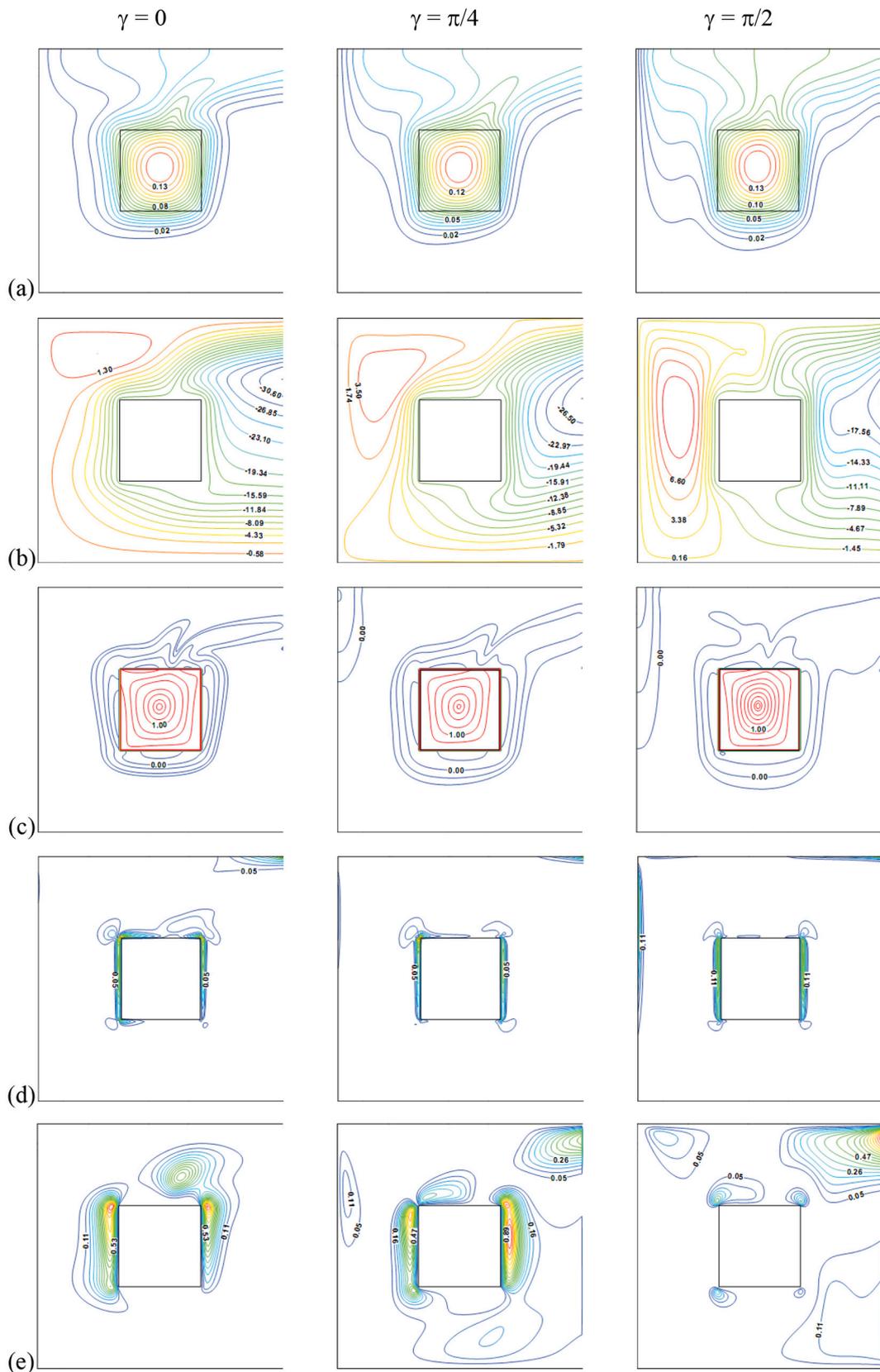
Fig. 4. Patterns of θ (a), Ψ (b), S_T (c), S_F (d) and S_M (e) for $k^* = 1.0$, $\phi = 0.04$, $\Omega = 0.01$ and $Ha = 50$ with various γ.

$\gamma = 0$ $\gamma = \pi/4$ $\gamma = \pi/2$
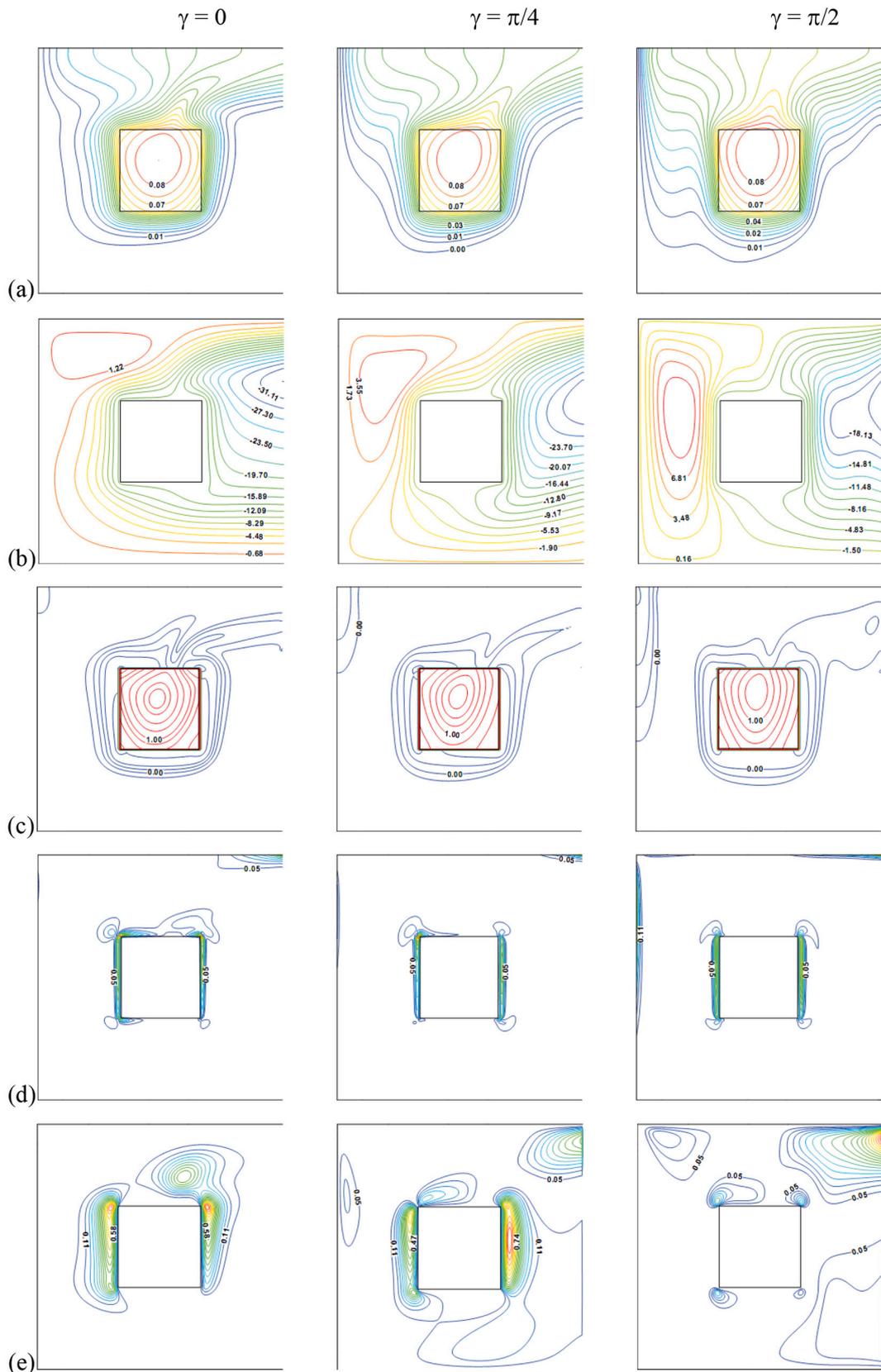
Fig. 5. Patterns of θ (a), Ψ (b), S_T (c), S_F (d) and S_M (e) for $k^* = 5.0$, $\phi = 0.04$, $\Omega = 0.01$ and $Ha = 50$ with various γ.
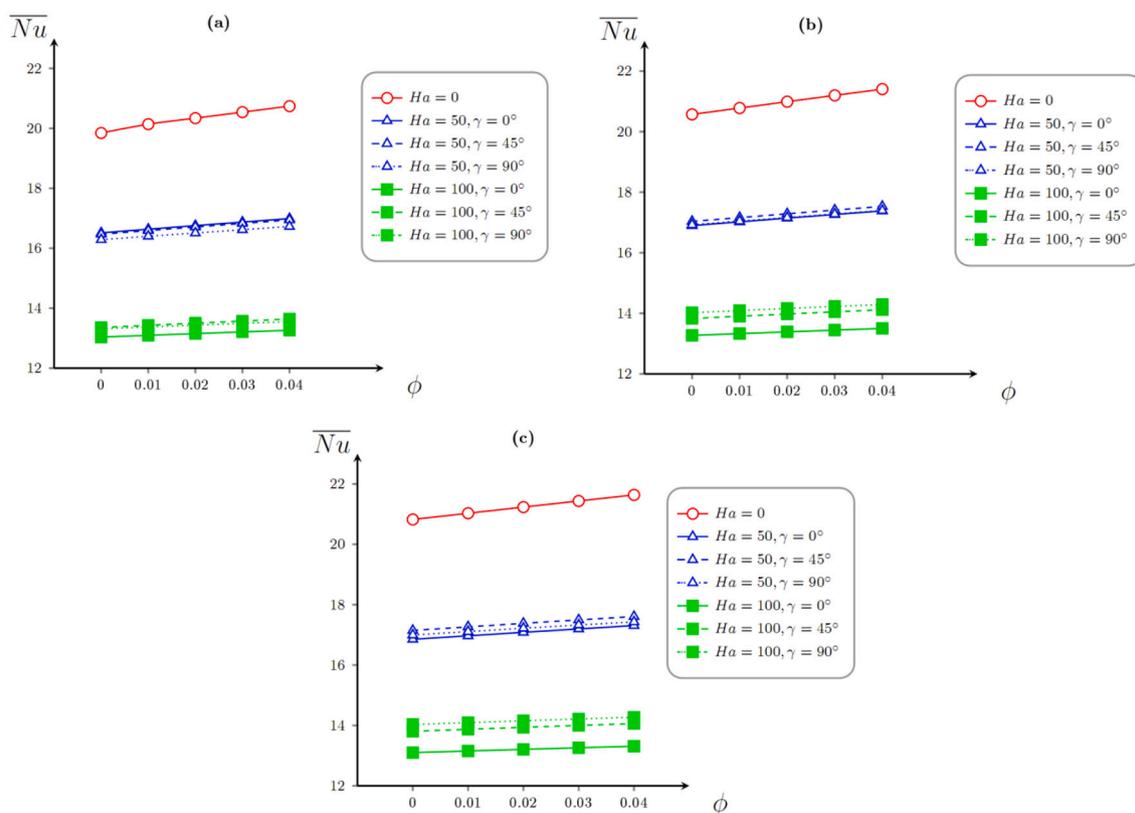
Fig. 6. Mean *Nu* change with ϕ for (a) $k^* = 0.1$, (b) $k^* = 1.0$, (c) $k^* = 5.0$ and various *Ha* and γ.

of the heat generating block provided significant effects in the overall entropy production and the vertical surfaces of the thermally-generating body which facing inlet and outlet of the cavity having maximum energy transport intensity. *Al*-Rashed et al. [33] examined mixed convective transport with the second law of thermodynamics in a nanosuspension vented 3D cavity with isothermal solid body in its center. The obtained data illustrated that *Be* and motion rate are increased with the increase of body length. The entropy generation is improved by the heat transport for high *Ri*. A computational study is investigated by Bondarenko et al. [34] on the mixed convective heat transference in a nanosuspension region with moved wall having the energy-producing body. They ascertained that high *Re* and central placed heated block provide better cooling to the entire domain.

Hussain et al. [35] investigated mixed convective energy transferences in a horizontal duct having an opened chamber containing insulated square block saturated with Al_2O_3-Cu nanosuspension. Their analysis demonstrated that the enhanced thermal transference and entropy production occur with raising *Ri*, *Re* and the nanoadditives concentration. They also found that for small values of *Ha*, the thermal transference irreversibility is influencing than the liquid friction irreversibility. You et al. [36] reported a constructed examination of energy transport in a non-uniform energy-producing triangular region and also computationally studied the entropy production performance. They introduced entropy generation drop concept into the constructed plan of triangular structures with both non-uniform energy production and discrete changeable cross sectional high conductive channels, that help to the plan of electronic gadget to a propitious energy transport. Tayebi et al. [37] explored the thermogravitational energy transport with a second law of thermodynamics for hybrid nanosuspension elliptical chamber having inner energy production or absorption. Their data demonstrated that the combined influence of inner energy production/absorption and hybrid nanosuspension essentially change the flow and temperature patterns, energy transport strength, and entropy production inside the domain of interest. Numerical analysis of free convective

energy transport combined with second law of thermodynamics for 3D opened chambers with an insulated diamond shaped block was performed by Kolsi et al. [38]. It was ascertained that an insulated diamond shaped body is used to dominate the energy transport, fluid flow and thermal regulation inside the system. Mahmoudi et al. [39] scrutinized entropy generation caused by thermogravitational energy transport in a partially opened domain having various locations of thin energy element subjected to a copper-water nanosuspension. Authors demonstrated that effective energy transport and liquid circulation occur when the opened boundary is located upper but the total entropy production is reverse function in this case. Sivaraj et al. [40] computationally scrutinized thermogravitational energy transport combined with the second law of thermodynamics for ferrofluid in a closed chamber with a solid block. Authors ascertained that increasing temperature difference reduces the entropy production intensity and addition of nanoparticles improves the heat transport and the entropy generation. Other interesting results can be found in [41–44].

The promising application of open cavity with heat generation is electronic devices. In order to keep the devices within an acceptable temperature, an efficient thermal management system will be needed to dissipate the heat generation. So that the primary objective of this investigation is to analyze MHD free convective transport combined with the second law of thermodynamics for an opened cavity filled with ferrofluid under heat producing solid body effect. The present project deals with an influence of the different heat conductivity ratio of solid block, angle of inclined Lorentz force and temperature differences on the entropy production.

2. Mathematical formulation

MHD thermogravitational heat transference combined with the second law of thermodynamics for an opened domain of length *L* with the center placed energy-producing solid block of size *l* inside the cavity have been investigated. A scheme of the cavity is demonstrated in Fig. 1.
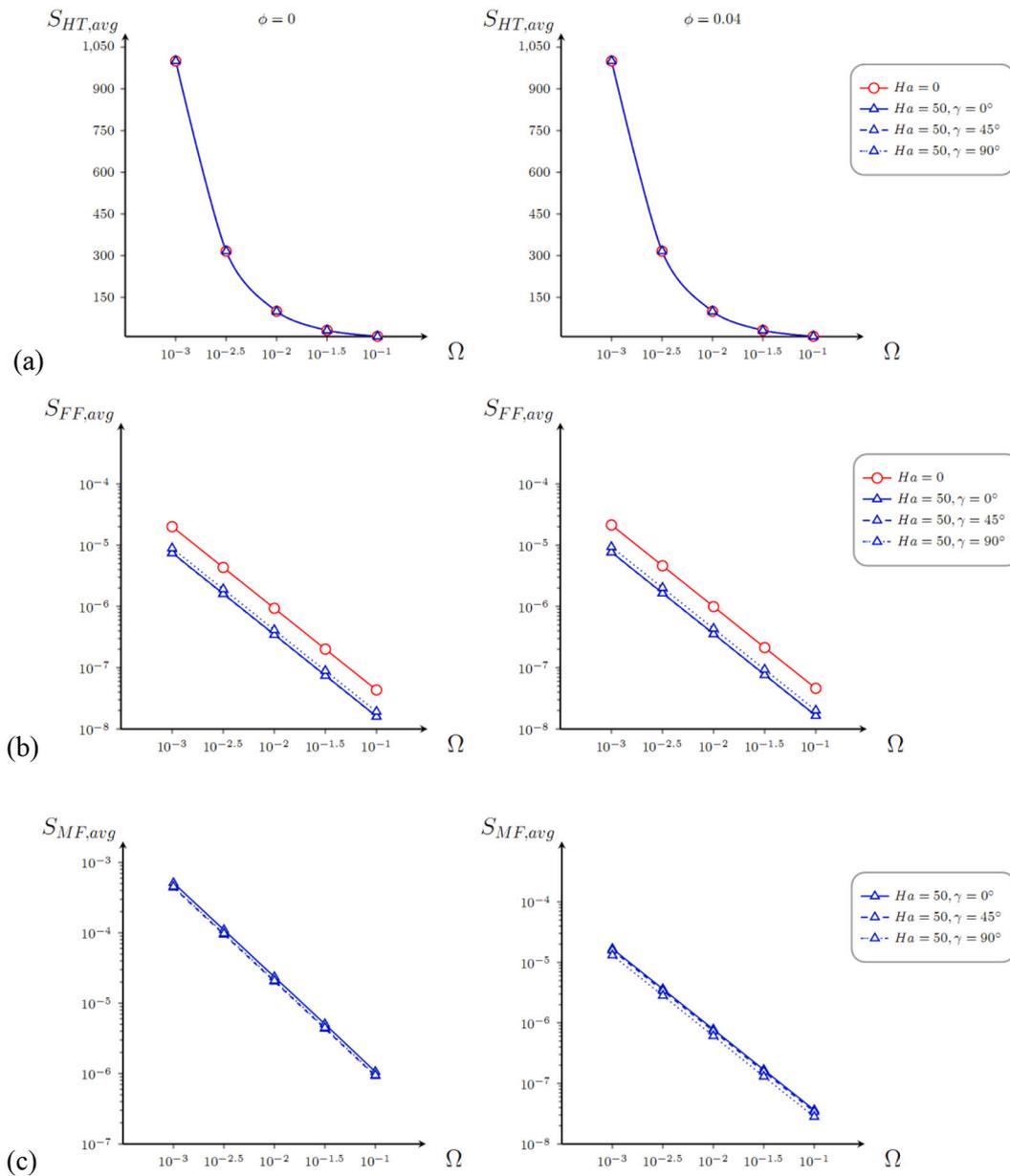
Fig. 7. Average entropy generation induced by (a) heat transport, (b) nanosuspension friction, (c) magnetic field with Ω for $k^* = 0.1$, different Ha and γ (left column is for $\phi = 0$, right column is for $\phi = 0.04$).

The inner body area is $L^2/9$ and it generates the heat with uniform rate q'''. The considered cavity has an isothermally cooling left wall while horizontal walls are adiabatic. An ambient cold nanofluid can penetrate into the lower portion of right side of the cavity and it also can exit upper portion from the same side. The nanosuspension includes nanosized spherical ferrous oxide and the physical parameters are in Table 1. The considered nanosuspension is Newtonian and the thermal equilibrium conditions are valid. The liquid circulation and energy transport are laminar, while the Boussinesq approximation is used. Further, the angle of the tilted magnetic field B is defined by γ. The induced magnetic influence is neglected in comparison with the applied Lorentz force.

Under the formulated conditions, the energy, momentum and mass transport is described as [15,40,41].

$$\frac{\partial u}{\partial x} + \frac{\partial v}{\partial y} = 0 \tag{1}$$

$$\frac{\partial u}{\partial t} + u\frac{\partial u}{\partial x} + v\frac{\partial u}{\partial y} = -\frac{1}{\rho_{nf}}\frac{\partial p}{\partial x} + \frac{\mu_{nf}}{\rho_{nf}}\left(\frac{\partial^2 u}{\partial x^2} + \frac{\partial^2 u}{\partial y^2}\right) + \frac{\sigma_{nf}}{\rho_{nf}}B^2[v \cdot cos(\gamma) - u \cdot sin(\gamma)]sin(\gamma) \tag{2}$$

$$\frac{\partial v}{\partial t} + u\frac{\partial v}{\partial x} + v\frac{\partial v}{\partial y} = -\frac{1}{\rho_{nf}}\frac{\partial p}{\partial y} + \frac{\mu_{nf}}{\rho_{nf}}\left(\frac{\partial^2 v}{\partial x^2} + \frac{\partial^2 v}{\partial y^2}\right) + \frac{(\rho\beta)_{nf}}{\rho_{nf}}g(T - T_c) +$$
$$+\frac{\sigma_{nf}}{\rho_{nf}}B^2[u \cdot sin(\gamma) - v \cdot cos(\gamma)]cos(\gamma) \tag{3}$$

$$\frac{\partial T}{\partial t} + u\frac{\partial T}{\partial x} + v\frac{\partial T}{\partial y} = \alpha_{nf}\left(\frac{\partial^2 T}{\partial x^2} + \frac{\partial^2 T}{\partial y^2}\right) \tag{4}$$

$$(\rho c_p)_s\frac{\partial T}{\partial t} = k_s\left(\frac{\partial^2 T}{\partial x^2} + \frac{\partial^2 T}{\partial y^2}\right) + q''' \tag{5}$$

subjected to the additional limitations
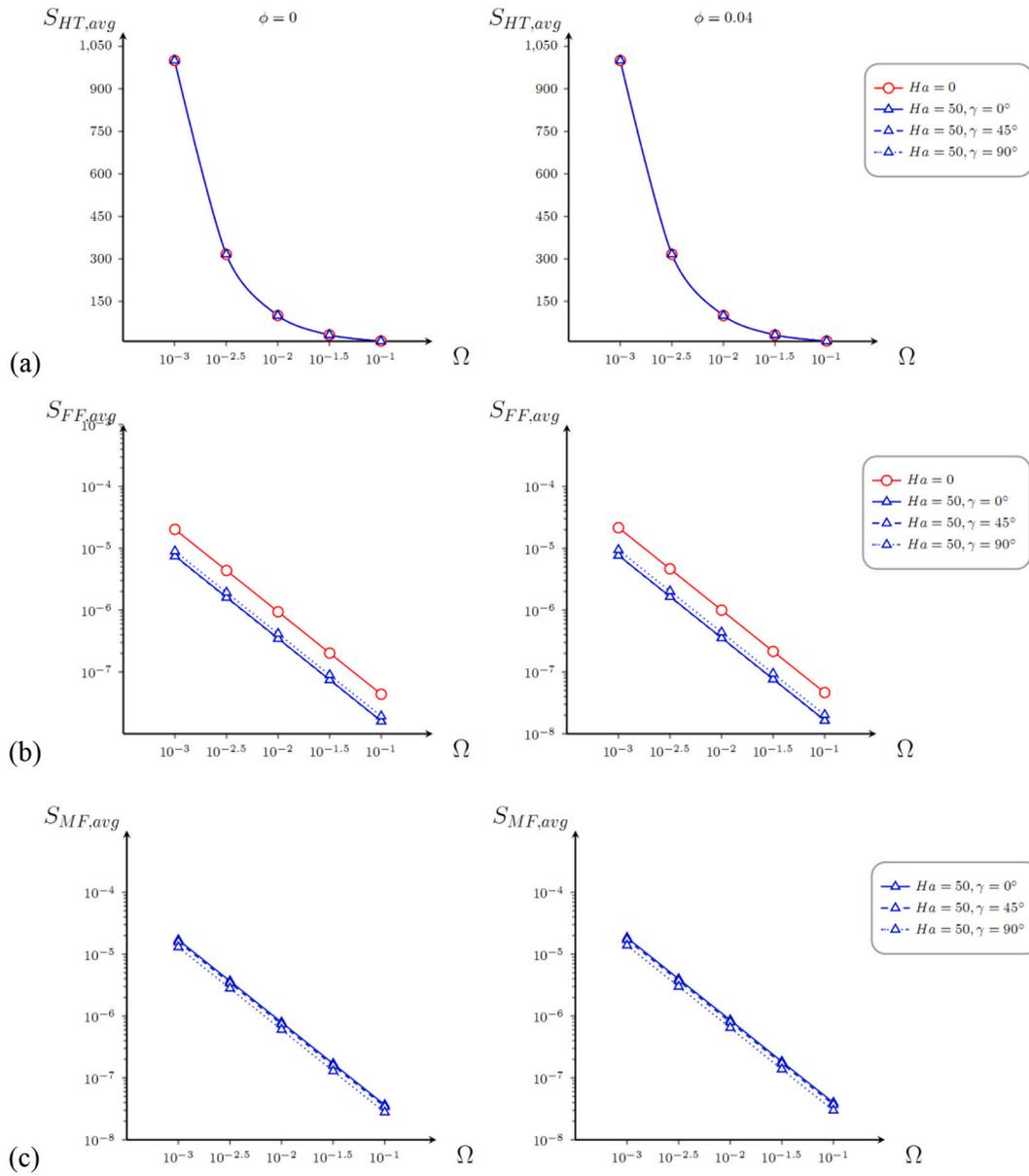
Fig. 8. Average entropy generation induced by (a) heat transport, (b) nanosuspension friction, (c) magnetic field with Ω for $k^* = 1.0$, different Ha and γ (left column is for $\phi = 0$, right column is for $\phi = 0.04$).

$$t = 0: \quad u = v = 0, T = T_c \quad \text{at } 0 \leq x \leq L \text{ and } 0 \leq y \leq L;$$

$$t > 0: \quad u = v = 0, T = T_c \quad \text{at the left wall;}$$

$$u = v = 0, \frac{\partial T}{\partial y} = 0 \quad \text{at the bottom} \Big/ \text{top walls;}$$

$$\frac{\partial u}{\partial x} = -\frac{\partial v}{\partial y}, \frac{\partial v}{\partial x} = 0, \frac{\partial T}{\partial x}\Big|_{out} = 0, T_{in} = 0 \quad \text{at the right opening;}$$

$$u = v = 0, k_{nf}\frac{\partial T}{\partial \eta} = k_s\frac{\partial T}{\partial \eta} \quad \text{at the fluid} \Big/ \text{solid interface.}$$

(6)

The considered nanoliquid effective density (ρ_{nf}), thermal diffusivity (α_{nf}), specific heat ($\rho c_p)_{nf}$, thermal expansion coefficient (β_{nf}), thermal conductivity (k_{nf}), viscosity (μ_{nf}) and electrical conductivity (σ_{nf}) are obtained by [47,48].

The above governing equations can be non-dimensionalized employing the parameters

$$X = \frac{x}{L}, \quad Y = \frac{y}{L}, \quad U = \frac{uL}{\alpha_f}, \quad V = \frac{vL}{\alpha_f}, \quad P = \frac{pL^2}{\rho_{nf}\alpha_f^2}, \quad \tau = \frac{t\alpha_f}{L^2}, \quad \theta = \frac{T - T_c}{\Delta T}, \quad \Delta T = \frac{q'''l^2}{k_f}$$

(7)
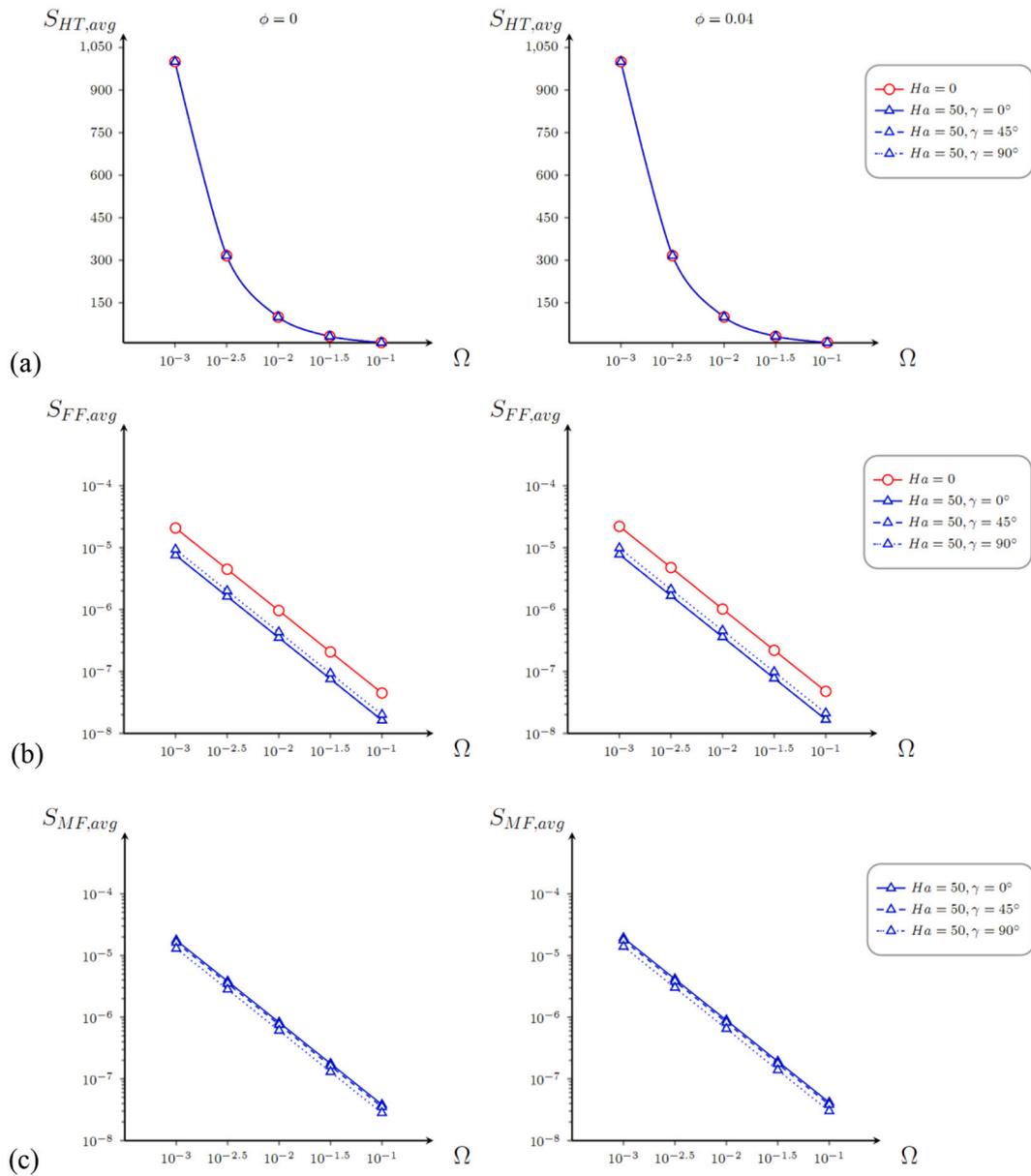
Fig. 9. Average entropy generation induced by (a) heat transport, (b) nanosuspension friction, (c) magnetic field with Ω for $k^* = 5.0$, different Ha and γ (left column is for $\phi = 0$, right column is for $\phi = 0.04$).

Table 6
Nanosuspension flow rate, entropy generation induced by the heat transport, nanoliquid friction and magnetic field for $\Omega = 0.01$, $\phi = 0.04$ and different k^*, Ha and γ.

k^*	Ha	γ	$|\Psi|_{max}$	$S_{gen,T,max}$	$S_{gen,F,max}$	$S_{gen,M,max}$
	0		57.7845	909.427	$4.730 \cdot 10^{-5}$	–
0.1		0	31.8246	909.206	$2.127 \cdot 10^{-5}$	$1.579 \cdot 10^{-5}$
	50	$\pi/4$	27.4303	909.397	$3.228 \cdot 10^{-5}$	$8.689 \cdot 10^{-6}$
		$\pi/2$	20.0269	909.461	$3.114 \cdot 10^{-5}$	$1.123 \cdot 10^{-5}$
	0		58.3133	900.587	$4.715 \cdot 10^{-5}$	–
1.0		0	32.0210	900.421	$2.127 \cdot 10^{-5}$	$1.551 \cdot 10^{-5}$
	50	$\pi/4$	27.7476	900.55	$3.284 \cdot 10^{-5}$	$9.436 \cdot 10^{-6}$
		$\pi/2$	20.2970	900.596	$3.080 \cdot 10^{-5}$	$1.122 \cdot 10^{-5}$
	0		59.7721	900.238	$4.865 \cdot 10^{-5}$	–
5.0		0	32.5304	900.234	$2.177 \cdot 10^{-5}$	$1.619 \cdot 10^{-5}$
	50	$\pi/4$	28.6040	900.288	$3.384 \cdot 10^{-5}$	$1.060 \cdot 10^{-5}$
		$\pi/2$	20.9599	900.29	$3.009 \cdot 10^{-5}$	$1.121 \cdot 10^{-5}$

The non-dimensional transport Eqs. (1)–(5) were formulated as [15,40,41].

$$\frac{\partial U}{\partial X} + \frac{\partial V}{\partial Y} = 0 \tag{8}$$

$$\frac{\partial U}{\partial \tau} + U\frac{\partial U}{\partial X} + V\frac{\partial U}{\partial Y} = -\frac{\partial P}{\partial X} + \left(\frac{\mu_{nf}\rho_f}{\mu_f\rho_{nf}}\right)Pr\left(\frac{\partial^2 U}{\partial X^2} + \frac{\partial^2 U}{\partial Y^2}\right) +$$
$$+ \left(\frac{\sigma_{nf}\rho_f}{\sigma_f\rho_{nf}}\right)Ha^2 Pr[V \cdot cos(\gamma) - U \cdot sin(\gamma)]sin(\gamma) \tag{9}$$

$$\frac{\partial V}{\partial \tau} + U\frac{\partial V}{\partial X} + V\frac{\partial V}{\partial Y} = -\frac{\partial P}{\partial Y} + \left(\frac{\mu_{nf}\rho_f}{\mu_f\rho_{nf}}\right)Pr\left(\frac{\partial^2 V}{\partial X^2} + \frac{\partial^2 V}{\partial Y^2}\right) + \left(\frac{(\rho\beta)_{nf}}{\rho_{nf}\beta_f}\right)RaPr\theta +$$
$$+ \left(\frac{\sigma_{nf}\rho_f}{\sigma_f\rho_{nf}}\right)Ha^2 Pr[U \cdot sin(\gamma) - V \cdot cos(\gamma)]cos(\gamma) \tag{10}$$

$$\frac{\partial \theta}{\partial \tau} + U\frac{\partial \theta}{\partial X} + V\frac{\partial \theta}{\partial Y} = \frac{\alpha_{nf}}{\alpha_f}\left(\frac{\partial^2 \theta}{\partial X^2} + \frac{\partial^2 \theta}{\partial Y^2}\right) \tag{11}$$

$$\left(\rho c_p\right)^*\frac{\partial \theta}{\partial \tau} = k^*\left(\frac{\partial^2 \theta}{\partial X^2} + \frac{\partial^2 \theta}{\partial Y^2}\right) + \frac{1}{A^*} \tag{12}$$

Corresponding non-dimensional limitations are

$\tau = 0: \quad U = V = 0, \theta = 0$ at $0 \le X \le 1$ and $0 \le Y \le 1$;

$\tau > 0: \quad U = V = 0, \theta = 0$ at $X = 0$;

$$U = V = 0, \frac{\partial \theta}{\partial Y} = 0 \text{ at } Y = 0 \text{ and } Y = 1;$$

$$\frac{\partial U}{\partial X} = -\frac{\partial V}{\partial Y}, \frac{\partial V}{\partial X} = 0, \frac{\partial \theta}{\partial X}\Big|_{out} = 0, \theta_{in} = 0 \text{ at } X = 1; \tag{13}$$

$$U = V = 0, \frac{\partial \theta}{\partial \eta} = k^*\frac{\partial \theta}{\partial \eta} \text{ at the fluid}\Big/\text{solid interface}$$

Dimensionless numbers included in Eqs. (8–12) are

$$Pr = \frac{\nu_f}{\alpha_f}, \ Ra = \frac{g\beta_f\Delta TL^3}{\nu_f\alpha_f}, \ Ha = BL\sqrt{\frac{\sigma_f}{\mu_f}}, \ k^* = \frac{k_s}{k_{nf}}, \ A^* = \frac{l^2}{L^2}, \ \left(\rho c_p\right)^*$$

$$= \frac{\left(\rho c_p\right)_s}{\left(\rho c_p\right)_{nf}} \tag{14}$$

Definition of the stream function Ψ is

$$U = \frac{\partial \Psi}{\partial Y}, \ V = -\frac{\partial \Psi}{\partial X} \tag{15}$$

Thermal performance is expressed by the local Nusselt number (*Nu*) given for each border of the heat-generating body as

$$Nu = \frac{k_{nf}}{k_f}\frac{\partial \theta}{\partial n} \tag{16}$$

Thus, integrating Eq. (16) we get the mean Nusselt number $\left(\overline{Nu}\right)$.

In this work irreversibility is affected by thermal transport, liquid friction, and Lorentz force impact. The overall entropy is the addition of the irreversibilities induced by the temperature gradient, nanosuspension friction and Lorentz force as follows [49–52].

$$\overline{s_{gen}} = \overline{s_T} + \overline{s_F} + \overline{s_M} \tag{17}$$

where entropy generation induced by heat transport $(\overline{s_T})$, nanosuspension friction $(\overline{s_F})$ and Lorentz force influence $(\overline{s_M})$ can be defined as follows,

$$\overline{s_T} = \overline{s_{T,f}} + \overline{s_{T,s}} \tag{18}$$

where $\overline{s_{T,f}}$ and $\overline{s_{T,s}}$ are defined as follows.

$$\overline{s_{T,f}} = \frac{k_{nf}}{T^2}\left[\left(\frac{\partial T}{\partial x}\right)^2 + \left(\frac{\partial T}{\partial y}\right)^2\right] \text{ for nanofluid} \tag{19}$$

$$\overline{s_{T,s}} = \frac{k_s}{T^2}\left[\left(\frac{\partial T}{\partial x}\right)^2 + \left(\frac{\partial T}{\partial y}\right)^2\right] + \frac{q_{gen}'''}{T} \text{ for the solid phase} \tag{20}$$

$$\overline{s_F} = \frac{\mu_{nf}}{T}\left[2\left(\frac{\partial u}{\partial x}\right)^2 + 2\left(\frac{\partial v}{\partial y}\right)^2 + \left(\frac{\partial u}{\partial y} + \frac{\partial v}{\partial x}\right)^2\right] \tag{21}$$

$$\overline{s_M} = B^2\frac{\sigma_{nf}}{T}\left[u\cdot sin(\gamma) - v\cdot cos(\gamma)\right]^2 \tag{22}$$

In Eq. (20), $\frac{q_{gen}'''}{T}$ represents as solid phase heat transfer contributes to irreversibility.

These equations have been non-dimensionlized and irreversibility components are

$$S_{gen} = S_T + S_F + S_M \tag{23}$$

Entropy generation induced by the heat transport is indicated as

$$S_T = \overline{s_T}\cdot\frac{T_c^2 L^2}{k_f\Delta T^2} \tag{24}$$

$$S_T = S_{T,f} + S_{T,s} \tag{25}$$

where,

$$S_{T,f} = \frac{k_{nf}}{k_f}\frac{1}{\Omega^2\left(\theta + \Omega^{-1}\right)^2}\left[\left(\frac{\partial \theta}{\partial X}\right)^2 + \left(\frac{\partial \theta}{\partial Y}\right)^2\right] \text{ for nanofluid} \tag{26}$$

$$S_{T,s} = \frac{k^*}{\Omega^2\left(\theta + \Omega^{-1}\right)^2}\left[\left(\frac{\partial \theta}{\partial X}\right)^2 + \left(\frac{\partial \theta}{\partial Y}\right)^2\right] + \frac{1}{A^*}\frac{1}{\Omega^2\left(\theta + \Omega^{-1}\right)} \text{ for the solid phase} \tag{27}$$

Entropy generation induced by the nanosuspension friction is identified as

$$S_F = \overline{s_F}\cdot\frac{T_c^2 L^2}{k_f\Delta T^2} \tag{28}$$

$$S_F = \frac{\mu_{nf}}{\mu_f}\frac{1}{\Omega^2\left(\theta + \Omega^{-1}\right)}\frac{Ge}{Ra}\left[2\left(\frac{\partial U}{\partial X}\right)^2 + 2\left(\frac{\partial V}{\partial Y}\right)^2 + \left(\frac{\partial U}{\partial Y} + \frac{\partial V}{\partial X}\right)^2\right] \tag{29}$$

Entropy generation induced by the Lorentz force is expressed as

$$S_M = \overline{s_M}\cdot\frac{T_c^2 L^2}{k_f\Delta T^2} \tag{30}$$

$$S_M = \frac{\sigma_{nf}}{\sigma_f}\frac{1}{\Omega^2\left(\theta + \Omega^{-1}\right)}\frac{Ge}{Ra}Ha^2[U\cdot sin(\gamma) - V\cdot cos(\gamma)]^2 \tag{31}$$

In the above Eqs. (25)–(31) one can find non-dimensional characteristics such as

$$\Omega = \frac{\Delta T}{T_c} \text{ and } Ge = \frac{g\beta_f L}{(c_p)_f} \tag{32}$$

The mean non-dimensional entropy production ($S_{gen,\ avg}$) is

$$S_{gen,avg} = \int_A S_{gen}\ dA = S_{T,avg} + S_{F,avg} + S_{M,avg} \tag{33}$$

Here $S_{T,\ avg}$, $S_{F,\ avg}$, $S_{M,\ avg}$ are average entropy production induced by the heat transport, liquid friction and magnetic field respectively.

Bejan number illustrating the ratio of entropy generation induced by the energy transport to the overall entropy generation is given as follows [49,52].

$$Be = S_T\big/S_{gen} \tag{34}$$

The average Bejan number is specified as

$$Be_{avg} = S_{T,avg}\big/S_{gen,avg} \tag{35}$$

3. Numerical technique and validation

Finite volume method was taken to work out Eqs. (8)–(12) combined with limitations in Eqs. (13). The diffusion terms are adopted by the central differences, while the power law scheme [53] was adopted to approximate the convective members to make the computational procedure stable. To develop the computational code FORTRAN language has been used. Combination of the pressure and velocity fields is performed employing SIMPLE procedure [53,54]. The Thomas algorithm is used to get solution of algebraic equations. The convergence criteria was assumed in the following form

$$\frac{\sum_{i,j}\left|\phi_{i,j}^m - \phi_{i,j}^{m-1}\right|}{\sum_{i,j}\left|\phi_{i,j}^m\right|} \le 10^{-7} \tag{36}$$

where ϕ represents *U*, *V* or θ and *m* is the iteration parameter respectively.

The precision of the computation is confirmed by comparing the solutions with a benchmark on free convection in an opened chamber which was analyzed by other authors. A fine accordance between current solution with literatures is shown in Table 2.

Suppose the entropy generation is studied, a matching is done with the problem on free convection combined with the second law of thermodynamics for a region with an isothermal partition [43]. Table 3 gives the overall entropy generation obtained numerically for $Ra = 10^5$, $h_1 = 0.5$ and different Ω.

The computational code was also verified with published data of House et al. [55]. The average Nusselt number for various heat conductivity ratio (k^*), heat generation body size (ζ) and the Rayleigh number (Ra) is shown in Table 4.

The mesh sensitivity analysis was conducted using various grids of 62×62, 122×122, 182×182, 242×242 elements for the maximum stream function $|\Psi|_{max}$, and the results were presented in Table 5 for $Ra = 10^7$, $\phi = 0.04$, $k^* = 1$, and $Ha = 50$. For optimization and calculation correctness, the computational mesh size of 182×182 elements was adopted for the present analysis.

4. Results and discussion

In the present study, the inclined Lorentz force impact on natural convective energy transport and entropy production in a nanofluid opened chamber containing energy-producing solid element with size of *l* (1/3 *L*) at its center. Computational investigation was performed for following control parameters, namely, $Ra = 10^7$, $(\rho c_p)^* = 1$, $Pr = 6.8377$, $0 \leq \phi \leq 0.04$, $Ha = 0$–100, $\gamma = 0$–$\pi/2$, the heat conductivity parameter ($0 \leq k^* \leq 5$) and the dimensionless temperature difference ($\Omega = 0.001$–0.1). The area ratio A^* is 1/9 and the cooled border temperature is $T_c = 300$ K. The computational outcomes are explored employing patterns of temperature and stream function, normalized values of entropy contours and the Nusselt numbers.

Fig. 2 illustrates patterns of temperature, stream function and entropy induced by the heat transport and liquid friction at $\Omega = 0.01$ and $Ha = 0$ for nanosuspension ($\phi = 0.04$). Energy producing solid block is influenced by different thermal conductivity ratio k^*. As can been found, the cooled fluid penetrates the chamber from the right side bottom zone of the opened border, interacts with energy-producing element and then leaves the chamber from the upper half of the opened border. The temperature field reflects (Fig. 2a) an essential heating inside the solid body where it is more uniform with a raise of k^*. When $k^* = 5$ the heat generating body increases the amount of energy transported from the element to the nanosuspension. A development of isolines density close to the heat-generating body and exit portion of the open boundary can be found. Fig. 2b shows a penetration of nanofluid with cold temperature through the lower open boundary into the cavity. The length of the entering zone at $X = 1$ is greater than the length of the exit area at $X = 1$. The temperature of these flows close to the solid body rises and the nanosuspension becomes lighter and the liquid moves to the upper exit portion of the cavity. Due to temperature reduction at the left wall and warming at the energy-producing element a convective cell is formed at the left side of the cavity. Moreover, increasing in k^* contributes to an increasing in nanofluid circulation rate ($|\Psi|_{max}^{k_*=0.1} = 58.97 < |\Psi|_{max}^{k_*=5.0} = 60.97$).

Fig. 2c demonstrates the patterns of entropy production caused by the energy transport. Thermal contours increase considerably near the heat generating surfaces. This appearance caused by velocity field grew all over the surfaces of the heat generating body and also temperature within the solid body transfer heat to the nanofluid. Therefore, convective cooling of the surface is expected. Further it should be noted that the thermal contours extend into the cavity region. This indicates that conduction dominates against the convection cooling. The entropy

generation induced by the nanosuspension friction is relatively high close to the vertical and upper borders of the solid block and minor vortex appears in the top corners of heat generation body which is shown in Fig. 2d. An appearance of these velocity gradients due to cooling fluid contact with hot border of the solid block and it extends to the exit portion of the cavity. Also, a velocity gradient near the heat generating solid body is reduced while increases the thermal conductivity ratio (k^*).

Figs. 3–5 illustrate temperature and stream function as well as entropy contours caused by the heat transport, liquid friction and magnetic field for $Ha = 50$ with various tilted angles and different ϕ. An addition of magnetic field results to vital warming inside the cavity. The thickness of heat boundary layer is formed near the solid block due to an impact of Lorentz force which acts orthogonal to the applied magnetic field presented in Figs. 3a–5a for $\gamma = 0$.

A rise of angle of magnetic field to $\pi/4$ enhances the thermal transmission by pushing the thermal plume towards the exit portion of the open cavity. The distribution of temperature isolines is modified when the magnetic field orientation varies between $\gamma = 0$ and $\gamma = \pi/2$. Moreover, an increasing of thermal conductivity ratio (k^*), one can find a formation of significant heat boundary layer around the heat generating element and top area of the chamber. In the case of the streamlines presented Figs. 3b–5b one convective cell is occurred left side of the cavity and another one attributes an intrusion of nanofluid from the open boundary inside the region. An occurrence of the convective cell near the left cold wall is described by the creation of thermal difference between the cold wall and heat generation body. Therefore, this circulation shows a counter-clockwise flow of nanofluid. A growth of magnetic intensity results to reduction of their propagation in the flow domain. Also, the increasing angle of inclined magnetic field between $\gamma = 0$ and $\gamma = \pi/2$ leads to increasing the left side counter-rotating cells. At the same time, it is feasible to conclude that an increment of k^* results to the improvement of convective recirculation between the heater and the left wall.

An entropy generation induced by the energy transport is presented in Figs. 3c–5c. An interaction of left convective cell with penetrative flow for the open border makes a temperature gradient around the solid body. One can find that the heat boundary layer is appeared at upper left of the cavity owing to above mentioned counter-clockwise rotating vortex. In particular for $\gamma = \pi/2$ one can find an increment of the size of the heat boundary layer over the cold vertical left border. With further raising of k^*, entropy generation due to heat transference increases more because of the excessive temperature difference at the element. Accordingly, for Figs. 3d–5d the entropy generation induced by the nanosuspension friction is found at vertical and upper surfaces of the heat-generating solid body.

Since the flow field attains higher velocity in these areas as compared to the remaining portion of the chamber. The inclusion of the Lorentz force reduces the fluid friction entropy lines due to less velocity gradient. Moreover, for $\gamma = \pi/2$ the fluid flow along the vertical wall incidents the effects of the attenuation from the Lorentz force which produces low thickness of velocity boundary layers there. There is an increment in the fluid friction entropy lines as thermal conductivity ratio changes its value from 0.1 to 5.0. Figs. 3e–5e illustrate the entropy contours due to a magnetic field effect occurring in closed proximity to the vertical border of the solid block. This is due to an occurrence of horizontal magnetic field. When increasing the magnetic inclination angle, one can find the vortex near the left vertical and exit area of the chamber. In particular the magnetic field is applied vertically ($\gamma = \pi/2$), the vortex near the vertical surface of a solid body deformed and occupied the corners of the solid body, because the magnetic entropy lines are substantial on the horizontal flow regions of the cavity. In entropy contours there are no significant changes while increasing the heat conductivity ratio (k^*) of the heat generating solid body. An inclusion of ferrous oxide nanoadditives in the base fluid results to quite significant modification of streamlines and isotherms. This modification

helps to intensified cooling process inside the system and there are no essential variations of entropy generations.

Fig. 6 illustrates the change of mean *Nu* at the solid block surfaces with ϕ for various k^*, *Ha* and γ. It is evident that mean *Nu* raises with nanoadditives concentration (ϕ) and thermal conductivity ratio (k^*). The observation also shows that growth of *Ha* decreases the convective motion strength, so that the cooling performance reduces as evidenced by Nusselt number of the surfaces of heat generating solid body. Moreover, the higher energy transport can be found for $k^* = 5$. Figs. 7–9 demonstrate the modification of mean entropy production induced by heat transport, liquid friction and magnetic field with Ω for different k^*, ϕ, *Ha* and γ. Entropy contours rate decreases as temperature difference increases for all considered values of k^*. The average entropy generation induced by the Lorentz force is found to be maximum when $Ha = 50$ and $γ = 0$. Further raising the magnetic inclination angle to at $γ = π/2$ characterizes an increment of entropy fluid friction (see Figs. 7b–9b). At the same time, it is diminishing the entropy production caused by the Lorentz force. A raise of the thermal conductivity ratio results to slight growth of entropy generation induced by the heat transport, nano-suspension friction and magnetic field (See Table 6). Also, Figs. 7–9 show that an impact of ferrous oxide is effective in diminution of energy transport intensity for high *Ra*. Moreover, there are quite differences in the parameters of the entropy generation due to the nanosuspension friction and Lorentz force.

5. Conclusions

This research deals with MHD thermogravitational transport combined with the second law of thermodynamics for a square open ferro-fluid cavity having a heat generating solid body. For fixed Rayleigh number ($Ra = 10^7$), computational analysis is performed for different ϕ, k^*, *Ha*, γ and Ω. The calculated results are demonstrated that,

- An increasing effect of magnetic field weakened the fluid motion rate, mean *Nu* and mean entropy generations.
- The inclination angle of magnetic field effect shows the higher mean *Nu*. When $γ = π/2$ the entropy generation induced by the heat transport and liquid friction attains higher values but the entropy production caused by the Lorentz force has the minimum value for all considered k^*.
- For all k^*, the mean *Nu* and average entropy generation are raised with nanoadditives concentration.
- The maximum heat transfer rate occurs at high thermal conductivity ratio ($k^* = 5.0$), while the minimum entropy production occurs at low thermal conductivity ratio ($k^* = 0.1$).
- An increment of temperature drop (Ω) leads to decrease in the mean entropy generation induced by the heat transport, nanosuspension friction and magnetic field for all k^*. Therefore, for a better cooling influence, rising thermal conductivity of the internal energy-producing solid block and nanoadditives concentration is productive impact.

Declaration of Competing Interest

None.

Acknowledgments

References

[1] Y. Xie, S. Shi, J. Tang, H. Wu, J. Yu, Experimental and analytical study on heat generation characteristics of a lithium-ion power battery, Int. J. Heat Mass Transf. 122 (2018) 884–894.

[2] S.M. Aminossadati, B. Ghasemi, A numerical study of mixed convection in a horizontal channel with a discrete heat source in an open cavity, Eur. J. Mech. B/Fluids 28 (2009) 590–598.

[3] S.Z. Shuja, M.O. Iqbal, B.S. Yilbas, Natural convection in a square cavity due to a protruding body- aspect ratio consideration, Heat Mass Transf. 37 (2001) 361–369.

[4] M.M. Rahman, S. Parvin, N.A. Rahim, M.R. Islam, R. Saidur, M. Hasanuzzaman, Effects of Reynolds and Prandtl number on mixed convection in a ventilated cavity with a heat-generating solid circular block, Appl. Math. Model. 36 (2012) 2056–2066.

[5] D.K. Singh, S.N. Singh, Conjugate free convection with surface radiation in open top cavity, Int. J. Heat Mass Transf. 89 (2015) 444–453.

[6] I.V. Miroshnichenko, M.A. Sheremet, H.F. Oztop, N. Abu-Hamdeh, Natural convection of Al₂O₃/H₂O nanofluid in an open inclined cavity with a heat-generating element, Int. J. Heat Mass Transf. 126 (2018) 184–191.

[7] M.A. Sheremet, H.F. Oztop, D.V. Gvozdyakov, M.E. Ali, Impacts of heat-conducting solid wall and heat-generating element on free convection of Al₂O₃/H₂O nanofluid in a cavity with open border, Energies 11 (2018) 1–17.

[8] A.H. Mahmoudi, M. Shahi, A.M. Shahedin, N. Hemati, Numerical modeling of natural convection in an open cavity with two vertical thin heat sources subjected to a nanofluid, Int. Commun. Heat Mass Transfer 38 (2011) 110–118.

[9] J.Y. Oh, M.Y. Ha, K.C. Kim, Numerical study of heat transfer and flow of natural convection in an enclosure with a heat generating conducting body, Numer. Heat Transfer A 31 (1996) 289–303.

[10] A. Raisi, Heat transfer in an enclosure filled with a nanofluid and containing a heat-generating conductive body, Appl. Therm. Eng. 110 (2017) 469–480.

[11] E.V. Shulepova, M.A. Sheremet, H.F. Oztop, N. Abu-Hamdeh, Mixed convection–radiation in lid-driven cavities with nanofluids and time-dependent heat-generating body, J. Therm. Anal. Calorim. 146 (2021) 725–738.

[12] S. Saravanan, C. Sivaraj, Combined thermal radiation and natural convection in a cavity containing a discrete heater: effects of nature of heating and heater aspect ratio, Int. J. Heat Fluid Flow 66 (2017) 70–82.

[13] S.A. Mikhailenko, M.A. Sheremet, A.A. Mohamad, Convective-radiative heat transfer in a rotating square cavity with a local heat-generating source, Int. J. Mech. Sci. 142-143 (2018) 530–540.

[14] I. Pop, M.A. Sheremet, T. Grosan, Thermal convection of nanoliquid in a double-connected chamber, Nanomaterials 10 (2020) 1–16.

[15] C. Sivaraj, V. Miroshnichenko, M.A. Sheremet, Influence of thermal radiation on thermogravitational convection in a tilted chamber having heat-producing solid body, Int. Commun. Heat Mass Transfer 115 (2020) 104611.

[16] A. Purusothaman, K. Murugesan, A.J. Chamkha, 3D modeling of natural convective heat transfer from a varying rectangular heat generating source, J. Therm. Anal. Calorim. 138 (2019) 597–608.

[17] T. Tayebi, H.F. Öztop, A.J. Chamkha, MHD natural convection of a CNT-based nanofluid-filled annular circular enclosure with inner heat-generating solid cylinder, Eur. Phys. J. Plus 150 (2021) 1–21.

[18] K.M. Gangawane, MHD free convection in a partially heated open-ended square cavity: effect of angle of magnetic field and heater location, Int. J. Appl. Comput. Math. 63 (2019) 1–19.

[19] M.A. Abbassi, Lattice Boltzmann method for simulation of nanoparticle Brownian motion and magnetic field effects on free convection in a nanofluid-filled open cavity with heat generation/absorption, Fluid Dynam. Mater. Process. 13 (2017) 59–83.

[20] A. Mahmoudi, I. Mejri, M.A. Abbassi, A. Omri, Analysis of MHD natural convection in a nanofluid-filled open cavity with non uniform boundary condition in the presence of uniform heat generation/absorption, Powder Technol. 269 (2015) 275–289.

[21] D. Prakash, N. Elango, I.S. Hussain, Effect of heat generation on MHD free convective flow of viscous fluid in a vertical channel in the presence of variable properties, AIP Conf. Proc. 2277 (2020), 030016.

[22] M.M. Rahman, M.M. Billah, N.A. Rahim, R. Saidur, M. Hasanuzzaman, Finite element simulation of magnetohydrodynamic mixed convection in a double-lid driven enclosure with a square heat-generating block, J. Heat Transf. 134 (2012), 062501.

[23] C. Sivaraj, M.A. Sheremet, MHD natural convection in an inclined square porous cavity with a heat conducting solid block, J. Magn. Magn. Mater. 426 (2017) 351–360.

[24] A.I. Alsabery, M.A. Ismael, A.J. Chamkha, I. Hashim, Effects of two-phase nanofluid model on MHD mixed convection in a lid-driven cavity in the presence of conductive inner block and corner heater, J. Therm. Anal. Calorim. 135 (2019) 729–750.

[25] V.M. Job, S.R. Gunakala, Mixed convection nanofluid flows through a grooved channel with internal heat generating solid cylinders in the presence of an applied magnetic field, Int. J. Heat Mass Transf. 107 (2017) 133–145.

[26] S.E. Ahmed, M.A. Mansour, A.K. Hussein, B. Mallikarjuna, M.A. Almeshaal, L. Kolsi, MHD mixed convection in an inclined cavity containing adiabatic obstacle and filled with Cu–water nanofluid in the presence of the heat generation and partial slip, J. Therm. Anal. Calorim. 138 (2019) 1443–1460.

[27] C. Revnic, T. Grosan, I. Pop, D.B. Ingham, Magnetic field effect on the unsteady free convection flow in a square cavity filled with a porous medium with a constant heat generation, Int. J. Heat Mass Transf. 54 (2011) 1734–1742.

[28] M.M. Ali, R. Akhter, M.A. Alim, Hydromagnetic natural convection in a wavy-walled enclosure equipped with hybrid nanofluid and heat generating cylinder, Alexandria Eng. J. 60 (2021) 5245–5265.

[29] S.C. Saha, Effect of MHD and heat generation on natural convection flow in an open square cavity under microgravity condition, Eng. Comput. Int. J. Comput.-Aided Eng. Software 30 (2013) 5–20.

[30] S.Z. Shuja, B.S. Yilbas, Entropy generation due flow passing over the porous block in the cavity, Prog. Comput. Fluid Dynam. 15 (2015) 16–24.

[31] S.R. Hosseini, M. Ghasemian, M. Sheikholeslami, A. Shafee, Z. Li, Entropy analysis of nanofluid convection in a heated porous microchannel under MHD field considering solid heat generation, Powder Technol. 344 (2019) 914–925.

[32] S.Z. Shuja, B.S. Yilbas, M.O. Budair, Natural convection in a square cavity with a heat generating body: entropy consideration, Heat Mass Transfer 36 (2000) 343–350.

[33] A.A.A.A. Al-Rashed, K. Kalidasan, L. Kolsi, R. Velkennedy, A. Aydi, A.K. Hussein, E.H. Malekshah, Mixed convection and entropy generation in a nanofluid filled cubical open cavity with a central isothermal block, Int. J. Mech. Sci. 135 (2017) 362–375.

[34] D.S. Bondarenko, M.A. Sheremet, H.F. Oztop, M.E. Ali, Impacts of moving wall and heat-generating element on heat transfer and entropy generation of Al$_2$O$_3$/H$_2$O nanofluid, J. Therm. Anal. Calorim. 136 (2019) 673–686.

[35] S. Hussain, S.E. Ahmed, T. Akbar, Entropy generation analysis in MHD mixed convection of hybrid nanofluid in an open cavity with a horizontal channel containing an adiabatic obstacle, Int. J. Heat Mass Transf. 114 (2017) 1054–1066.

[36] J. You, H. Feng, L. Chen, Z. Xie, Constructal design of nonuniform heat generating area based on triangular elements: a case of entropy generation minimization, Int. J. Therm. Sci. 139 (2019) 403–412.

[37] T. Tayebi, H.F. Öztop, A.J. Chamkha, Natural convection and entropy production in hybrid nanofluid filled-annular elliptical cavity with internal heat generation or absorption, Therm. Sci. Eng. Prog. 19 (2020) 100605.

[38] L. Kolsi, O. Mahian, H.F. Oztop, W. Aich, M.N. Borjini, N. Abu-Hamdeh, H.B. Aissia, 3D buoyancy-induced flow and entropy generation of nanofluid-filled open cavities having adiabatic diamond shaped obstacles, Entropy 18 (2016) 1–17.

[39] A.H. Mahmoudi, M. Shahi, F.T. Semnan, I.R. Iran, Entropy generation due to natural convection in a partially open cavity with a thin heat source subjected to a nanofluid, Numer. Heat Transfer A 61 (2012) 283–305.

[40] C. Sivaraj, S. Priyadharsini, M.A. Sheremet, Thermal convection and entropy generation of ferrofluid in an enclosure containing a solid body, Int. J. Numer. Methods Heat Fluid Flow 31 (9) (2021) 2940–2961.

[41] C. Sivaraj, V.E. Gubin, A.S. Matveev, M.A. Sheremet, Impacts of uniform magnetic field and internal heated vertical plate on ferrofluid free convection and entropy generation in a square chamber, Entropy 23 (2021) 709.

[42] M. Famouri, K. Hooman, Entropy generation for natural convection by heated partitions in a cavity, Int. Commun. Heat Mass Transfer 35 (2008) 492–502.

[43] Y.L. Chan, C.L. Tien, A numerical study of two-dimensional natural convection in square open cavities, Numer. Heat Transfer 8 (1985) 65–80.

[44] J.F. Hinojosa, R.E. Cabanillas, G. Alvarez, C.E. Estrada, Nusselt number for the natural convection and surface thermal radiation in a square tilted open cavity, Int. Commun. Heat Mass Transfer 32 (2005) 1184–1192.

[45] K.M. Rabbi, S. Saha, S. Mojumder, M.M. Rahman, R. Saidur, T.A. Ibrahim, Numerical investigation of pure mixed convection in a ferrofluid-filled lid-driven cavity for different heater configurations, Alexandria Eng. J. 55 (2016) 127–139.

[46] M. Sheikholeslami, D.D. Ganji, Ferrohydrodynamic and magnetohydrodynamic effects on ferrofluid flow and convective heat transfer, Energy 75 (2014) 400–410.

[47] T. Javed, M.A. Siddiqui, Effect of MHD on heat transfer through ferrofluid inside a square cavity containing obstacle/heat source, Int. J. Therm. Sci. 125 (2018) 419–427.

[48] N.S. Gibanov, M.A. Sheremet, H.F. Oztop, K. Al-Salem, Effect of uniform inclined magnetic field on natural convection and entropy generation in an open cavity having a horizontal porous layer saturated with a ferrofluid, Numer. Heat Transfer A 72 (2017) 479–494.

[49] A. Bejan, Entropy generation minimization, CRC Press, Boca Raton, 1996.

[50] A. Sciacovelli, V. Verda, E. Sciubba, Entropy generation analysis as a design tool – a review, Renew. Sust. Energ. Rev. 43 (2015) 1167–1181.

[51] T.W. Ting, Y.M. Hung, N. Guo, Entropy generation of viscous dissipative nanofluid convection in asymmetrically heated porous microchannels with solid-phase heat generation, Energy Conv. Manage. 105 (2015) 731–745.

[52] C. Sivaraj, E. Vignesh, M.A. Sheremet, Entropy generation in MHD free convection of nanoliquid within a square open chamber with a solid body, Int. J. Numer. Methods Heat Fluid Flow (2021), https://doi.org/10.1108/HFF-03-2021-0172.

[53] S.V. Patankar, Numerical Heat Transfer and Fluid Flow, Hemisphere Publishing Corporation, 1980.

[54] J.P. Van Doormaal, G.D. Raithby, Enhancements of the SIMPLE method for predicting incompressible fluid flows, Numer. Heat Transfer A 7 (1984) 147–163.

[55] J.M. House, C. Beckemann, T.E. Smith, Effect of a centered conducting body on natural convection heat transfer in an enclosure, Numer. Heat Transfer A 18 (1990) 213–225.